Video Article

Ligand-Mediated Nucleation and Growth of Palladium Metal Nanoparticles

Saeed Mozaffari*[1], Wenhui Li*[1], Coogan Thompson[1], Sergei Ivanov[2], Soenke Seifert[3], Byeongdu Lee[4], Libor Kovarik[5], Ayman M. Karim[1]

[1]Department of Chemical Engineering, Virginia Polytechnic Institute and State University

[2]Center for Integrated Nanotechnologies, Los Alamos National Laboratory

[3]Advanced Photon Source, Argonne National Laboratory

[4]X-ray Science Division, Argonne National Laboratory

[5]Environmental Molecular Science Laboratory, Pacific Northwest National Laboratory

*These authors contributed equally

Correspondence to: Ayman M. Karim at amkarim@vt.edu

URL: https://www.jove.com/video/57667
DOI: doi:10.3791/57667

Keywords: Chemistry, Issue 136, Ligands, palladium, nucleation and growth, kinetic modeling, ligand-based model, LaMer, size control, small angle X-ray spectroscopy

Date Published: 6/25/2018

Citation: Mozaffari, S., Li, W., Thompson, C., Ivanov, S., Seifert, S., Lee, B., Kovarik, L., Karim, A.M. Ligand-Mediated Nucleation and Growth of Palladium Metal Nanoparticles. *J. Vis. Exp.* (136), e57667, doi:10.3791/57667 (2018).

Abstract

The size, size distribution and stability of colloidal nanoparticles are greatly affected by the presence of capping ligands. Despite the key contribution of capping ligands during the synthesis reaction, their role in regulating the nucleation and growth rates of colloidal nanoparticles is not well understood. In this work, we demonstrate a mechanistic investigation of the role of trioctylphosphine (TOP) in Pd nanoparticles in different solvents (toluene and pyridine) using *in situ* SAXS and ligand-based kinetic modeling. Our results under different synthetic conditions reveal the overlap of nucleation and growth of Pd nanoparticles during the reaction, which contradicts the LaMer-type nucleation and growth model. The model accounts for the kinetics of Pd-TOP binding for both, the precursor and the particle surface, which is essential to capture the size evolution as well as the concentration of particles *in situ*. In addition, we illustrate the predictive power of our ligand-based model through designing the synthetic conditions to obtain nanoparticles with desired sizes. The proposed methodology can be applied to other synthesis systems and therefore serves as an effective strategy for predictive synthesis of colloidal nanoparticles.

Video Link

The video component of this article can be found at https://www.jove.com/video/57667/

Introduction

Controlled synthesis of metallic nanoparticles is of great importance due to the large applications of nanostructured materials in catalysis, photovoltaic, photonics, sensors, and drug delivery[1,2,3,4,5]. To synthesize the nanoparticles with specific sizes and size distribution, it is vital to understand the underlying mechanism for the particle nucleation and growth. Nevertheless, obtaining nanoparticles with such criteria has challenged the nano-synthesis community due to the slow progress in understanding the synthesis mechanisms and the lack of robust kinetic models available in the literature. In 1950s, LaMer proposed a model for the nucleation and growth of sulfur sols, where there is a burst of nucleation followed by a diffusion-controlled growth of nuclei[6,7]. In this proposed model, it is postulated that the monomer concentration increases (due to the reduction or decomposition of the precursor) and once the level is above the critical supersaturation, the energy barrier for particle nucleation can be overcome, resulting in a burst nucleation (homogeneous nucleation). Owing to the proposed burst nucleation, the monomer concentration drops and when it falls below the critical supersaturation level, the nucleation stops. Next, the formed nuclei are postulated to grow via the diffusion of monomers towards the nanoparticles surface, while no additional nucleation events occur. This results in effectively separating the nucleation and growth in time and controlling the size distribution during the growth process[8]. This model was used to describe the formation of different nanoparticles including Ag[9], Au[10], CdSe[11], and Fe_3O_4[12]. However, several studies illustrated that the classical nucleation theory (CNT) cannot describe the formation of colloidal nanoparticles, in particular for metallic nanoparticles where the overlap of the nucleation and growth is observed[1,13,14,15,16,17]. In one of those studies, Watzky and Finke established a two-step mechanism for the formation of iridium nanoparticles[13], in which a slow continuous nucleation overlaps with a fast nanoparticle surface growth (where growth is autocatalytic). The slow nucleation and fast autocatalytic growth were also observed for different types of metal nanoparticles, such as Pd[14,15,18], Pt[19,20], and Rh[21,22]. Despite recent advances in developing nucleation and growth models[1,23,24,25], the role of the ligands is often ignored in the proposed models. Nevertheless, ligands are shown to affect the nanoparticles size[14,15,26] and morphology[19,27] as well as the catalytic activity and selectivity[28,29]. For example, Yang *et al.*[30] controlled the Pd nanoparticle size ranging from 9.5 and 15 nm by varying the concentration of trioctylphosphine (TOP). In the synthesis of magnetic nanoparticles (Fe_3O_4), the size noticeably decreased from 11 to 5 nm when the ligand (octadecylamine) to metal precursor ratio increased from 1 to 60. Interestingly, the size of Pt nanoparticles was shown to be sensitive to the chain length of amine ligands (*e.g.*, n-hexylamine and octadecylamine), where smaller nanoparticle size could be obtained using longer chain (*i.e.*, octadecylamine)[31].

The size alteration caused by different concentration and different types of the ligands is a clear evidence for the contribution of ligands in the nucleation and growth kinetics. Unfortunately, few studies accounted for the role of ligands, and in these studies, several assumptions were often made for the sake of simplicity, which in turn make these models applicable only for specific conditions[32,33]. More specifically, Rempel and co-workers developed a kinetic model to describe the formation of quantum dots (CdSe) in the presence of capping ligands. However, in their study, the binding of the ligand with nanoparticle surface is assumed to be at equilibrium at any given time[32]. This assumption might hold true when the ligands are in large excess. Our group recently developed a new ligand-based model[14] which accounted for the binding of capping ligands with both the precursor (metal complex) and the surface of nanoparticle as reversible reactions[14]. In addition, our ligand-based model could potentially be used in other metal nanoparticle systems, where the synthesis kinetics seem to be affected by the presence of the ligands.

In the current study, we use our newly developed ligand-based model to predict the formation and growth of Pd nanoparticles in different solvents including toluene and pyridine. For our model input, *in situ* SAXS was utilized to obtain the concentration of nanoparticles and size distribution during the synthesis. Measuring both the size and concentration of particles, complemented by kinetic modeling, allows us to extract more precise information on the nucleation and growth rates. We further demonstrate that our ligand-based model, which explicitly accounts for the ligand-metal binding, is highly predictive and can be used to design the synthesis procedures to obtain nanoparticles with desired sizes.

Protocol

1. Pd Acetate Recrystallization

CAUTION: This protocol involves hands-on operations with high temperature glassware and solution. Use personal protective equipment including goggles and heat-resistant gloves. All the operations involving solution handling should be conducted in a fume hood and avoid other heating sources nearby due to the corrosive and flammable properties of anhydrous acetic acid.

1. Add 40 mL of anhydrous acetic acid into a 50 mL three neck round bottom flask with 0.75 g of Pd acetate and a stir bar. Attach the condenser to the middle neck, cap the other two openings and fix the flask on the stirring hotplate.
2. Open the condensing water valve slowly and let the water flow through the condenser. Stir the solution for 10-15 min at 300 rpm at room temperature until no more Pd acetate can dissolve.
3. Set the hotplate temperature at 100 °C. After the temperature reaches 100 °C, wait for around 30 min until the Pd acetate completely dissolves.
4. During this time, pre-heat two 20 mL glass vials and all the filtration parts at 90 °C in a drying oven. Also, heat some water in a 500 mL beaker until it approaches the boiling point.
5. Quickly assemble the filtration parts and place the filter flask on a pre-heated hotplate (at 100 °C). Connect the vacuum pump to the filter flask. Quickly remove the three-neck round bottom flask from the hotplate and filter the Pd acetate solution under vacuum.
6. After the filtration, quickly pour the liquid into two 20 mL vials. Cap the vials and immerse them into the hot water in the beaker.
7. Put the beaker on a hotplate at 80 °C and slowly decrease the temperature to room temperature by decreasing the hotplate temperature by 20 °C every hour.
8. Turn off the hotplate after 3 h. Leave the beaker overnight for crystallization.
9. Pour the acetic acid out of the vials. Leave the Pd acetate trimer crystals in the vial. Wash the crystals for 3 times to remove the acetic acid residual by dispensing 2 mL of hexane evenly onto the crystals and then draining the solution.
10. Cover the vials with aluminum foil to avoid light. Dry the crystals under N_2 flow at room temperature overnight. Store the crystals in inert atmosphere.

2. Preparation for Pd Acetate – TOP Synthesis Solution[14]

1. Degas each solvent (pyridine, toluene or 1-hexanol) under N_2 flow at 10 mL/min for 30 min.
2. Weigh 0.0112 g of recrystallized Pd acetate for 2.5 mL of 20 mM solution in a 7 mL vial. Cap the vial, then purge and fill it with N_2 through the inlet on the septum with an inserted needle outlet.
3. Transfer the solvents and the Pd acetate vial into an N_2 glovebox. Add 2.5 mL of pyridine or toluene into the Pd acetate vial. Sonicate the vial for 40 min to dissolve all Pd acetate.
4. For each sample, transfer 1 mL of 20 mM Pd acetate solution into a 7 mL vial with a micro stir bar in the glovebox. Add 8.9 µL of trioctylphosphine (TOP:Pd molar ratio = 2) into the solution. Shake the vial for 30 s with hands to mix the agents well. Then, add 1 mL of 1-hexanol into each sample vial (solvent:hexanol = 50:50 in volume).

3. Colloidal Pd Nanoparticle Synthesis[14]

1. Pre-heat the hotplate with a heating insert at 100 °C. Purge the reaction vials with 10 mL/min of N_2 flowing above the solution level to create an inert atmosphere and a constant pressure.
2. Put the reaction vials in the pre-heated hotplate insert under 300 rpm stirring to start the reaction.
3. To terminate the reaction, remove the vials from the insert and cool the vials down to room temperature.

4. Pd Nanoparticle Characterization- *Ex situ* Small-angle X-ray Scattering (SAXS)[34]

1. **Mean size and size distribution characterization**
    1. Initialize the SAXS instrument. Click on the commander window in the measurement software and adjust the voltage and current to 50 kV and 1000 µA, respectively.
    2. Load the background solution (1:1 mixture of the solvent (pyridine or toluene) and 1-hexanol) into the capillary holder. Seal the capillary and fix it to the holder parallel to the X direction. Mount the holder inside the instrument chamber.

3. Start the vacuum pump and wait until the vacuum level in the chamber stabilizes (lower than 0.3 mbar).
4. Fix the X axis (along the capillary) and scan in the Y direction (across the capillary) to find the middle position as the measurement position, at which the X-ray pathway length through the liquid sample reaches the maximum (the diameter of the capillary).
5. Setup and run the wizard to conduct steps 4.1.5 – 4.1.8. Set the capillary position and mount the glassy carbon through the X-ray pathway so that the X-ray will go through the glassy carbon first and then the capillary. Take a measurement of 10 s and save the 2D scattering graph.
6. Move the glassy carbon out of the pathway. Take a measurement of 1800 s on the background solution and save the background scattering graph.
7. Move the capillary out of the pathway, mount the glassy carbon only and take a 10 s measurement.
8. Move the glassy carbon out of the pathway. Take a 10 s measurement of the black current (vacuum chamber only).
9. To measure the nanoparticle solution, load the sample into the capillary and follow the same procedures from 4.1.2 – 4.1.6.
10. For data analysis, open SAXS analysis software via **File | Import from file | Import the background and the sample files**.
11. Choose the 2D pattern of the background. Click **Indirect transmission calculation** in tool. Input the background with glassy carbon, glassy carbon and blank frame files and click on **OK**. Do the same operations on the sample pattern. The transmissions will be automatically calculated.
12. Drag the circle ring cursor from the edge to the center of the 2D scattering pattern to integrate the background and sample 2D graph to 1D scattering curve.
13. Choose the background curve in the list. Check it as background measurement in **SAXS information**.
14. Choose the background and the sample curves together. Right click and choose **Background correction** to subtract the background from the sample.
15. Right click on the curve after background correction. Choose **SAXS modeling | Directly modeling | Sphere | Schultz | No interaction**.
16. Set the Q range between 0.02 to 0.3. Click on **Initial guess** to give an estimation on the fitting results. Then click on **Fit** to fit the 1D SAXS curve with Schultz polydisperse sphere model to obtain the mean diameter r_{avg} and standard deviation σ (corresponding to the size distribution of the nanoparticles).

2. **Concentration of particles (N_p) extraction**
   1. Use the absolute intensity ($I(q)$), which can be correlated to both the size and concentration of nanoparticles in the solution as follows[14,35]:
   $$(1)\ I(q) = N_p \int_0^\infty f(r)\, V_p{}^2 P(q) dr$$
   where q is the scattering vector, N_p is the concentration of nanoparticles, V_p is the nanoparticle volume, and $P(q)$ is the single-particle form factor. Calculate the Schultz distribution factor[36] $f(r)$ in the case of polydisperse spherical shape nanoparticles using the following expression:
   $$(2)\ f(r) = \frac{r^z}{\Gamma(z+1)}\left[\frac{z+1}{r_{avg}}\right]^{z+1} \exp\left(-\frac{(z+1)r}{r_{avg}}\right)$$
   Here, $z = (r_{avg}/\sigma)^2 - 1$.
   2. Consider $q \to 0$, which is the extrapolation of the SAXS curve to the intercept to Y axis:
   $$(3)\ I(0) = N_p \langle V_p{}^2 \rangle (\Delta\rho)^2$$
   Δρ is the scattering length density difference between metal and solvent and $\langle V_p{}^2 \rangle$ is the average square of the particle volume.
   3. Calculate $\langle V_p{}^2 \rangle$ using equation:
   $$(4)\ \langle V_p{}^2 \rangle = \left(\frac{4\pi}{3}\right)^2 \int_0^\infty f(r)\, r^6 dr$$
   4. To obtain $I(0)$, use water (as a standard) to calibrate the scattering intensity to absolute scale due to its well-known absolute differential scattering cross-section of 1.632×10^{-2} cm^{-1} at room temperature[34]. Measure the empty capillary and water and subtract the empty capillary as a background for water following the procedures from 4.1.2 to 4.1.14.
   5. The 1D scattering curve for water is a straight line parallel to X-axis. Extrapolate the line to get the intercept intensity I_w (cm^{-1}) on Y-axis. Calculate the calibration factor (CF) as
   $= 1.632 \times 10^{-2} \mathrm{cm}^{-1}/I_w$.
   6. Find the extrapolation intensity $I_s(0)$ for the nanoparticle curves. Calibrate $I_s(0)$ to obtain $I(0)$ at absolute scale using the CF:
   $$(5)\ I(0) = CF \times I_s(q=0)$$
   7. Extract the concentration of the particles from the following equation derived from (3):
   $$(6)\ N_p = \frac{I(0)}{\langle V_p{}^2 \rangle (\Delta\rho)^2}$$

3. **Extraction of concentration of atoms in nanoparticles (Y) from *in situ* and *ex situ* SAXS**
   1. Use both the concentration of nanoparticles (N_p) and average value of number of atoms per nanoparticle (N_{ave}) to calculate the total concentration of atoms as discussed below.
   2. Calculate N_{ave} based on the following equation[37]:
   $$(7)\ N_{ave} = \frac{4\pi r^3 \rho N_A}{3M_w}$$

where *r* is the nanoparticle radius, N_A is the Avogadro's number, ρ is the metal density, and M_w is the metal molecular weight. For palladium, ρ = 12023 kg/m^3 and M_w = 0.1064 kg/mol.

3. To account for the size distribution in estimating the total concentration of atoms in nanoparticles, calculate the $\langle N_{ave} \rangle$ using equation (7) along with the Schultz distribution factor:

$$(8)\ \langle N_{ave} \rangle = \int_0^\infty \frac{4\pi r^3 \rho N_A}{3M_w} f(r)\, dr$$

4. Estimate the concentration of atoms (Y) through multiplying $\langle N_{ave} \rangle$ by the concentration of nanoparticles (N_p) at any given time as follows:

$$(9)\ Y = \frac{\langle N_{ave} \rangle}{N_A} \times N_p = \frac{4\pi\rho}{3M_w} N_p \int_0^\infty f(r)\, r^3 dr$$

5. Obtaining Kinetic Data from *in situ* SAXS on Colloidal Pd Nanoparticle Synthesis at Synchrotron

1. Before starting the reaction, take SAXS measurements on the empty capillary, capillary filled with water, and capillary filled with solvent:hexanol at 50:50.
2. Consider that the agent preparation procedures for *in situ* SAXS are the same with steps 1 and 2, except that the total reaction solution volume is 6 mL (10 mM $Pd(OAc)_2$ in 3 mL of pyridine or toluene mixed with 3 mL of 1-hexanol, with TOP:Pd molar ratio = 2).
3. In the glovebox, transfer the reaction solution into a 25 mL round bottom flask with a stir bar inside. Purge the space above the solution with N_2 (10 mL/min).
4. Set the stirring rate at 300 rpm. Put the flask in the pre-heated hotplate insert to trigger the reaction.
5. Take 300 µL of reaction solution into the capillary mounted through the X-ray beam path every 8 s using a programmed syringe pump. Collect the scattering data by the detector.
   Note: The transmission of the sample is directly measured by an ionized chamber (without glassy carbon). After each measurement, the solution is pumped back to the bulk reactor.
6. Consider that the data can be automatically converted to 1D curve with the beamline program. The mean diameter and standard deviation are obtained by fitting the data with Schultz polydisperse sphere model. The extraction of concentration of particles follows the same procedures in step 4.2 using the synchrotron X-rays.

6. Modeling Approach and Simulation Procedures for Nucleation and Growth of Palladium (Pd) Metal Nanoparticles

1. Consider the reduction and nucleation as one first-order pseudo-elementary reactions (equation (10)).
   Note: A pseudo-elementary reaction is defined as the sum of one (or more) slow elementary reactions followed by fast elementary reactions (non-rate determining reactions). Herein, the pseudo-elementary reaction represents the kinetics of the slow reaction(s), but have reaction orders equal to the stoichiometry of the sum reaction (hence, the term pseudo-elementary)[38]. For example, the corresponding reactions for $Pd(OAc)_2$ reduction and nucleation (TOP:Pd molar ratio=1) in the excess of 1-hexanol are presented below[15]:
   (i) $Pd(TOP)(OAc)_2(Solv) + R'CH_2OH \rightarrow Pd^0 + TOP + R'CHO + 2AcOH + Solv$ (overall ligand dissociation and reduction), which can be split into steps (ii) and (iii):
   (ii) $Pd(TOP)(OAc)_2(Solv) + Solv \rightarrow Pd(OAc)_2(Solv)_2 + TOP$ (Ligand dissociation)
   (iii) $Pd(OAc)_2(Solv)_2 + R'CH_2OH \rightarrow Pd^0 + R'CHO + 2AcOH + (Solv)_2$ (reduction)
   (iv) $n\ Pd^0 \rightarrow Pd^0_n$ (nucleation)
   The reduction (iii) and nucleation (iv) reactions are combined and shown as one pseudo-elementary reduction-nucleation step (A→B). Note that A represents the kinetically active precursor, and while it is written as $Pd(OAc)_2(Solv)_2$ in reaction (iii), other Pd complexes could be present.
2. Consider the surface growth of nanoparticles to be autocatalytic. Autocatalytic growth is one mode of growth which occurs through the reduction of precursor on the nanoparticle surface (equation (11))[37].
3. Account for the binding of capping ligands (TOP) with the precursor (which alter the precursor reactivity) as well as the surface of the particle.
   Note: The dissociation of the ligands (reverse reaction 12) was shown to be important for the nucleation of Ir nanoparticles[39].
   Additionally, other studies have shown that the ligands affect the precursor reactivity (reaction 12) as well as the growth rate of colloidal nanoparticles[14,15,16]. Include these reactions in the model (equations (12) and (13)) as two reversible reactions (neither is assumed to be equilibrated during the reaction)[14]. Note that our expansion of the FW mechanism[13] (reactions 10 and 11) accounted for the first time for the reversible binding of the ligands with both the precursor (reaction 12) and the surface of the nanoparticles (reaction 13).[14]
4. Assume the following reactions are pseudo-elementary.

$$(10)\ A \xrightarrow{k_{1-nuc}} B$$

$$(11)\ A + B \xrightarrow{k_{2-growth}} 2B$$

$$(12)\ A + L \underset{k_{3-f}, K_{5-eq}}{\rightleftarrows} AL$$

$$(13)\ B + L \underset{k_{4-f}, K_{6-eq}}{\rightleftarrows} BL$$

Here, k_{1-nuc} is the reduction/nucleation rate constant, $k_{2-growth}$ the surface growth rate constant, k_{3-f} the forward reaction rate constant for reaction (12), K_{5-eq} the equilibrium constant for ligand-metal precursor binding (i.e. reaction 12), k_{4-f} the forward reaction rate constant for reaction (13), and K_{6-eq} the equilibrium constant for the binding of ligand with the nanoparticle surface (i.e. reaction 13).

Note: In addition, *A* is representative of the kinetically active precursor, *L* the capping ligand (here TOP), *AL* the ligand–metal complex (here Pd(II)–TOP) which can be coordinated with different ligands (such as acetate, 1-hexanol or pyridine), *B* the uncapped Pd surface atom, and *BL* the Pd atom bound with ligand, Pd^0 –TOP. In addition, see the complete list for model description and assumptions in previous publication[14].

5. Calculate the concentration of Pd atoms (Y) from the kinetic model based on the following equation.

$$(14)\ Y = B + BL$$

6. Calculate the concentration of nanoparticles (N_p) from the model (if no evidence of agglomeration exists) as follows:

$$(15)\ N_p = \int_0^{t_r} \frac{k_{1-nuc}[A]}{n} N_A\, dt$$

Here, t_r is reaction time, $[A]$ the active precursor concentration, N_A Avogadro's number (6.022 x 10^{23}) and n the nucleus size (atoms/nucleus). n is selected to be "4" based on the smallest size detected during the reaction.

7. Use the following differential equations and initial conditions (in MATLAB) to obtain the concentration profile of different species.

Differential Equations:

$$(16)\ \frac{d[A]}{dt} = -k_{1-nuc}[A] - k_{2-growth}[A][B] - k_{3-f}[A][L] + \frac{k_{3-f}[AL]}{K_{5-eq}}$$

$$(17)\ \frac{d[B]}{dt} = k_{1-nuc}[A] + k_{2-growth}[A][B] - k_{4-f}[B][L] + \frac{k_{4-f}[BL]}{K_{6-eq}}$$

$$(18)\ \frac{d[L]}{dt} = -k_{3-f}[A][L] + \frac{k_{3-f}[AL]}{K_{5-eq}} - k_{4-f}[B][L] + \frac{k_{4-f}[BL]}{K_{6-eq}}$$

$$(19)\ \frac{d[AL]}{dt} = k_{3-f}[A][L] - \frac{k_{3-f}[AL]}{K_{5-eq}}$$

$$(20)\ \frac{d[BL]}{dt} = k_{4-f}[B][L] - \frac{k_{4-f}[BL]}{K_{6-eq}}$$

In addition, for the metal precursor and ligand concentrations (equations 21 and 22) at any given time "t", the following relationships can be written as follows:

$$(21)\ [A]_0 = [A]_t + [AL]_t$$

$$(22)\ [L]_0 = [L]_t + [AL]_t$$

$$(23)\ \frac{[AL]}{[A][L]} = K_{5-eq}\ \ (only\ at\ time = 0)$$

Note: Reaction (12), $A + L \xleftrightarrow{k_{3-f}, K_{5-eq}} AL$, is considered to be at equilibrium at time=0. After the reaction proceeds, the reaction is no longer constrained to be at equilibrium.

$$(24)\ [B]_0 = [BL]_0 = 0$$

8. Minimize the *SR* (*i.e.*, sum of normalized squared errors) between the experiments and model for N_p and Y using the MATLAB function fminsearch to extract the fitting parameters (rate constants shown in equations 10-13).

$$(25)\ SR = \min\left(\sum_{j=1}^{x}\left(\frac{N_p(\exp) - N_p(\text{model})}{N_p(\exp)}\right)^2 + \sum_{j=1}^{x}\left(\frac{Y(\exp) - Y(\text{model})}{Y(\exp)}\right)^2\right)$$

Here x is number of experimental data points.

9. Select similar distribution of the number of data points along the reaction time and Y-axis (N_p or Y) to make sure the minimization function is not weighted toward data points at early or later reaction times.

7. Obtaining Nucleation and Growth Rates from Both the Experimental Data and Model

1. Calculate the nucleation and growth rates from the model using the followings equations.

$$(26)\ \frac{dN_p}{dt} = \frac{k_{1-nuc}[A]}{n} N_A\ \left(\frac{number\ of\ nuclei}{L.s}\right)$$

$$(27)\ \frac{dN_{growth}}{dt} = k_{2-growth}[A][B]\ (mol.L^{-1}.s^{-1})$$

Here, $[N_{growth}]$ represents the concentration of atoms that contributed only to the particle growth.

Note: To make the unit of nucleation and growth rates the same (*i.e.*, $mol.L^{-1}.s^{-1}$), it is required to multiply equation (26) by $[n/N_A]$. This allows us to make a comparison between the rates.

2. Estimate the nucleation rate from the experimentally measured number of particles using short time intervals.

$$(28)\ \frac{dN_p}{dt} = \frac{\Delta N_p(\exp)}{\Delta t}$$

3. Estimate the growth rate by subtracting the contribution of nucleation from the total concentration of atoms ($Y\ (\exp)$) or metal precursor consumption. "$Y\ (\exp)$" quantifies both the formation of particles (nucleus) and particle growth.

$$(29)\ \frac{dN_{growth}}{dt} = \frac{\Delta Y(\exp)}{\Delta t} - \left(\frac{\Delta N_p(\exp)}{\Delta t} \times \frac{n}{N_A}\right)$$

Representative Results

To systematically examine whether the capping ligands alter the kinetics of nucleation and growth, we took the two following approaches: (i) the binding of the ligand with the metal was not considered in the kinetic model similar to previous studies (*i.e.*, the nucleation and autocatalytic growth) (ii) the reversible binding of capping ligand with the precursor and surface of the nanoparticle was taken into account in the model (*i.e.*, ligand-based model described in Protocol). Regarding the Pd synthesis in toluene, as shown in **Figure 1**, without accounting for the ligand-metal binding, the model failed to capture the time evolution of the nanoparticles concentration (N_p) and concentration of Pd atoms (Y). As an alternative, we implemented our newly developed kinetic model (**Figure 2**) and as depicted in **Figure 3**, the model accurately predicts our *in situ* data (both N_p and Y during reaction).This further indicates that the capping ligands indeed affect the nucleation and growth kinetics of Pd nanoparticles.

Estimating the rate constants (**Table 1**) from the model further enables us to obtain useful information on the kinetics of the nanoparticle formation. In this regard, **Figure 4A** shows the comparison between the nucleation and growth rates (as estimated from the model) and the results clearly reveal that nucleation is slow while the growth is fast, which agrees well with previous studies[1,14]. Both modeling and experimental results demonstrate that the metal precursor/monomer does not undergo burst nucleation. This is illustrated by the *in situ* SAXS and modeling results where the nucleation continues till the end of synthesis (**Figure 3B** and **Figure 4A**). The continuous formation of nuclei, therefore, contradicts the LaMer burst nucleation and growth model but supports the continuous nucleation reaction in the Finke-Watzky two step mechanism. In addition, the nucleation can be fitted by pseudo-first order; however, we cannot exclude the possibility that the nucleation could be higher in order. Herein, as shown in **Figure 4B**, the ligand plays a central role in the continuity of nucleation by further binding to the nanoparticle surface and reducing the concentration of active sites (*i.e.*, [*B*]). This drastically decreases the particle growth rate and expands the time window for the nucleation throughout the synthesis. In addition, our current results presented in this work in combination with our previous study[14] (where the synthesis was conducted under different experimental conditions) indicate that the ligand and precursor concentrations do not have a significant effect on the rate and equilibrium constants, which shows the chemical fidelity between the model and the real system.

Next, we probed the applicability of our ligand-based model to a different solvent system, where pyridine was used as a solvent instead of toluene. We can see that despite the significant difference observed for the nucleation and growth kinetics in pyridine compared to toluene (**Figure 5** and **Table 1**), the model accurately captures the *in situ* data, N_p and Y, and allows for more accurate estimation of rate constants (**Table 1**). One of the important features that makes a kinetic model robust is that it should be able to predict synthetic conditions for achieving nanoparticles with desired sizes. Therefore, we implemented our ligand-based model (using the same rate constants reported in **Table 1**) to predict the size under different concentrations of metal precursor, $Pd(OAc)_2$, in pyridine. **Figure 6** shows that the model can provide a very accurate estimation of the nanoparticle size under different concentrations of the metal precursor. The modeling as well as the experimental results demonstrate that the nanoparticles become larger in size at higher precursor concentration. This is because the growth is second order kinetics while the nucleation is first order which makes the growth faster at higher precursor concentration[14].

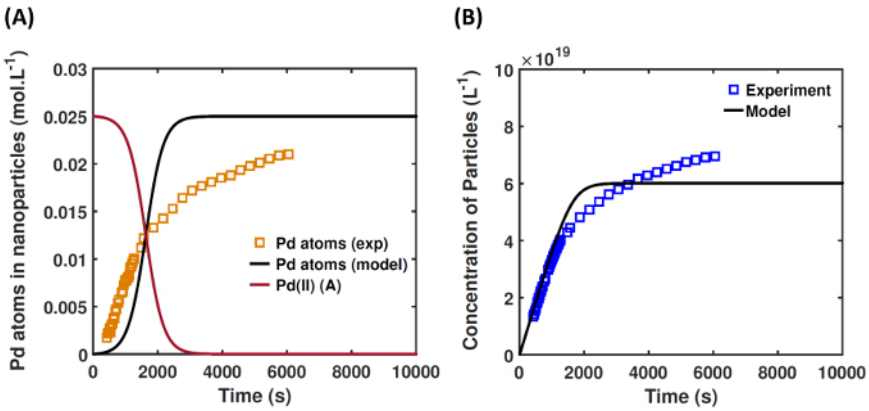

Figure 1. Experimental and two-step modeling results for the synthesis of Pd nanoparticles in toluene: (A) concentration of Pd atoms and (B) concentration of nanoparticles. The rate constants are $k_{1-nuc} = 0.98 \times 10^{-5} s^{-1}$ and $k_{2-growth} = 1.45 \times 10^{-1}$ L.mol^{-1}.s^{-1}. Experimental condition: [$Pd(OAc)_2$]=25 mM , TOP:Pd molar ratio= 2, and T (°C) = 100. Please click here to view a larger version of this figure.

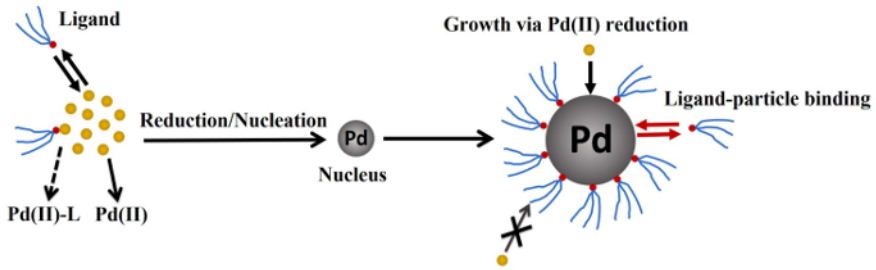

Figure 2. The schematic of ligand-mediated nucleation and growth model. In this proposed model, the capping ligands can associate and dissociate from both the metal precursor and nanoparticle surface, thereby, affecting the nucleation and growth kinetics (through altering the concentration of kinetically active precursor and the number of free surface sites, respectively). Please click here to view a larger version of this figure.

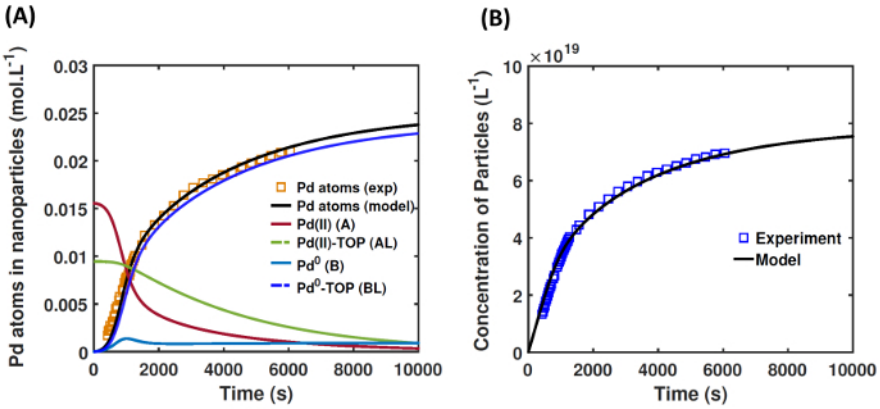

Figure 3. Experimental and ligand-based modeling results for the synthesis of Pd nanoparticles in toluene: (A) concentration of Pd atoms and (B) concentration of nanoparticles. The rate constants are summarized in **Table 1**. Experimental condition: $[Pd(OAc)_2]$=25 mM , TOP:Pd molar ratio= 2, and T (°C) = 100. Please click here to view a larger version of this figure.

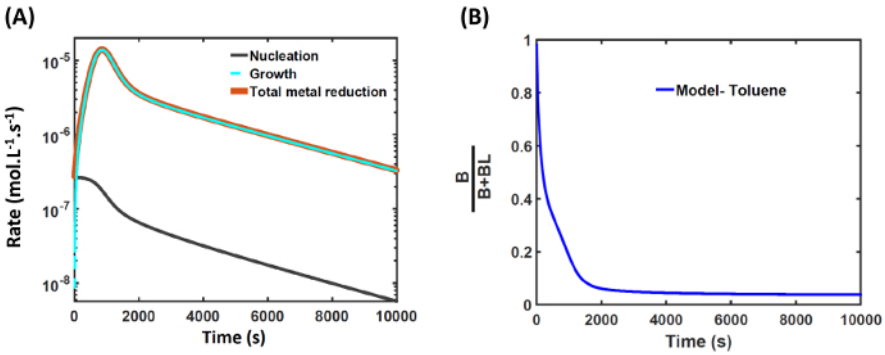

Figure 4. (A) The rates of the nucleation and growth extracted from the ligand-based model for the synthesis of Pd nanoparticles in toluene and (B) $\frac{B}{B+BL}$ ratio. Experimental condition: $[Pd(OAc)_2]$=25 mM , TOP:Pd molar ratio= 2, and T (°C) = 100. Please click here to view a larger version of this figure.

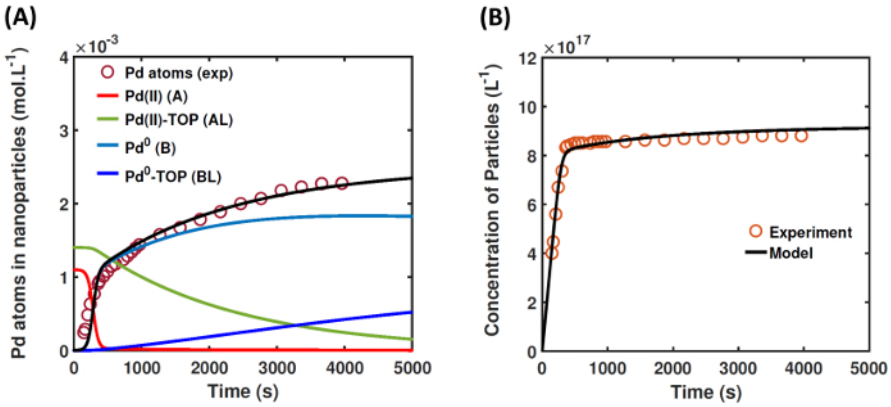

Figure 5. Experimental and ligand-based modeling results for the synthesis of Pd nanoparticles in pyridine: (A) concentration of Pd atoms and (B) concentration of nanoparticles. The rate constants are summarized in **Table 1**. Experimental condition: $[Pd(OAc)_2]$=2.5 mM , TOP:Pd molar ratio= 2, and T (°C) = 100. Please click here to view a larger version of this figure.

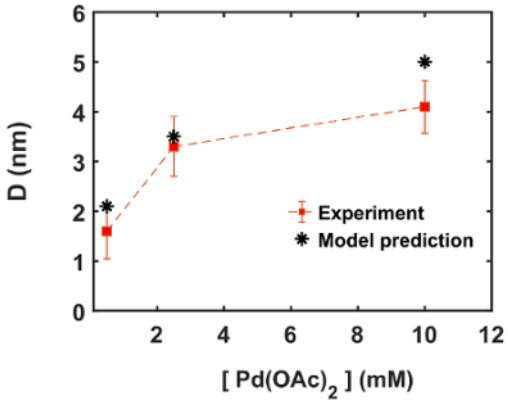

Figure 6. Model prediction of final nanoparticle size as a function of precursor concentration in pyridine solution (experimental data from Mozaffari *et al.*[14]). The error bars represent the standard deviation of the particle size distribution. Experimental condition: TOP:Pd molar ratio= 2, and T (°C) = 100. Please click here to view a larger version of this figure.

	$k_{1\text{-nuc}}$	$k_{2\text{-growth}}$	$k_{3\text{-f}}$ (A+L)	$k_{4\text{-f}}$ (B+L)	$K_{5\text{-eq}}$ (A+L)	$K_{6\text{-eq}}$ (B+L)
Units	s^{-1}	$L.mol^{-1}.s^{-1}$	$L.mol^{-1}.s^{-1}$	$L.mol^{-1}.s^{-1}$	$L.mol^{-1}$	$L.mol^{-1}$
25 mM Pd in Toluene	1.8×10^{-5}	10×10^{-1}	4.7×10^{-3}	3×10^{-1}	1.5×10^{1}	1×10^{3}
2.5 mM Pd in Pyridine	1.74×10^{-5}	2.34×10^{1}	1.7×10^{-1}	2.13×10^{-2}	3.54×10^{2}	1.44×10^{2}

Table 1. The extracted rate constants for Pd nanoparticle synthesis in different solvents (toluene and pyridine). Experimental condition: TOP:Pd molar ratio= 2, and T (°C) = 100.

Discussion

In this study, we presented a powerful methodology to examine the effect of capping ligands on the nucleation and growth of metal nanoparticles. We synthesized Pd nanoparticles in different solvents (toluene and pyridine) using Pd acetate as the metal precursor and TOP as the ligand.We used *in situ* SAXS to extract the concentration of reduced atoms (nucleation and growth events) as well as the concentration of nanoparticles (nucleation event), where both experimental observables were used as the model inputs. In addition, by considering the slope of the concentration of the nanoparticles and concentration of the atoms at the early reaction time, our methodology (the use of *in situ* SAXS and kinetic modeling), allowed us to estimate the upper and lower bonds for the nucleation and growth rate constants (more details can be found in ref. 14, which was the first study to decouple the contributions of nucleation and growth to the total metal reduction).

There are three critical steps in systematically examining the effects of ligand-metal binding on the nucleation and growth of colloidal nanoparticles: (i) measuring the evolution of size as well as the concentration of nanoparticles (steps 4.1-4.3). This is an important step as it can provide more detailed information on both the nucleation and growth events, (ii) developing a robust kinetic model, which explicitly accounts for the reactions of capping ligands with the metal and also includes the most relevant reactions during the formation and growth of nanoparticles (step 6.4), and (iii) constructing an appropriate link between the experimental observables and those extracted from the model (*e.g.*, size measured experimentally versus size extracted from the model).

It is important to note that due to the small size of the particles (< 10 nm in diameter), and the fast nucleation and growth rates in the beginning of the reaction, a high energy and high flux X-ray beam is needed for obtaining *in situ* data, which can be only realized at the synchrotron. Even with synchrotron beams, it is difficult to capture any size below 0.5 nm unless the concentration of the particle is high enough. A rule of thumb principle is that SAXS intensity reduces with 6^{th} power of the particle size but it is only linearly proportional to the concentration of the nanoparticles. In addition, for smaller nanoparticles, data acquisition up to much higher wave vector q (wider angle) is required, where the background scattering from solvents become more significantly detrimental to signal to noise ratio. This limits the size and concentration of small nanoparticles that can be detected in the early stages of the reaction, especially when the nucleation is slow and continuous as shown in this work. However, while the high energy/flux allows the acquisition of *in situ* data, the beam can also cause damage to the sample (agglomeration of nanoparticles and/or deposition on the cell walls). Therefore, in step 5.1, the beam energy and X-ray exposure time need to be tested and adjusted to the level that provides the best data quality (signal to noise ratio) for the detection of small nanoparticles in the early stages of the reaction without causing damage to the sample. The troubleshooting has to be done at the synchrotron during the *in situ* SAXS measurement, *i.e.*, to monitor the SAXS spectra and ensure that no agglomeration/precipitation occurs during the synthesis. Through a few tests, the beam energy was finally set at 18 keV with an appropriate exposure time (0.1 s) to capture enough signal, and hence, the small Pd nanoparticle size in the early stage of reaction. We also note that while the current kinetic model does not account for agglomeration, if such growth mechanism is dominant, the model can be modified to include agglomeration steps (for example, B + B → C and B + C → 1.5C, where B and C represent the small and larger nanoparticles, respectively)[1]. However, agglomeration as well as other modes of growth (*i.e.*, Ostwald and digestive ripening)[40] would be best described by population based models[24,25,32,33].

As already discussed in the manuscript, the underlying mechanism governing the nanoparticle nucleation and growth is poorly understood, particularly in the presence of coordinating ligands. For example, recent studies showed that TOP-Pd binding lowers the nucleation and growth rate of Pd nanoparticles[14,15,16,30]. Therefore, we accounted explicitly for the ligand-metal binding in our kinetic model. What distinguishes our method from other relevant studies is that our ligand-based model considers the ligand binding with both the precursor and surface of metal nanoparticle as reversible reactions and no *priori* assumptions are made on whether the ligands are in equilibrium with either of them. In addition, unlike previous studies where only one experimental observable (either size[33] or concentration of atoms[23], *etc.*) was used for model verification, our ligand-based model uses both the particle size and concentration of nanoparticles as model inputs. Therefore, it allows us to obtain more accurate estimates for the reaction rate and equilibrium constants.

Using our proposed methodology, we demonstrated the predictive power of our ligand-based model. In this regard, we showed that the model can predict the synthesis conditions to obtain nanoparticles with various sizes, which as a result minimizes the need for trial and error. Furthermore, with this simple "heat-up" synthesis method, the nanoparticle size can be tuned by changing the type of solvent or the metal concentration. These different sized Pd nanoparticles can have potential applications in catalysis, drug delivery, and sensors[15,41]. The presented synthesis strategy along with the kinetic modeling can be potentially used to provide insights on the role of capping ligands in the nucleation and growth of different types of nanoparticles to guide their controlled synthesis.

For future work, we direct our research toward developing kinetic models with the ability of predicting the size distribution during the synthesis. In addition, we will further investigate the validity of our ligand-based model under different experimental conditions, including different temperature ranges and different types of ligands and metals.

Disclosures

There is no conflict of interest to report.

Acknowledgements

The work was primarily funded by the National Science Foundation (NSF), Chemistry Division (award number CHE-1507370) is acknowledged. Ayman M. Karim and Wenhui Li acknowledge partial financial support by 3M Non-Tenured Faculty Award. This research used resources of the Advanced Photon Source (beamline 12-ID-C, user proposal GUP-45774), a U.S. Department of Energy (DOE) Office of Science User Facility operated for the DOE Office of Science by Argonne National Laboratory under Contract No. DE-AC02-06CH11357. The authors would like to thank Yubing Lu, a Ph.D. candidate in the Chemical Engineering Department at Virginia Tech for his kind help with the SAXS measurements. The presented work was partly executed at the Center for Integrated Nanotechnologies, an Office of Science User Facility operated for the U.S. Department of Energy (DOE) Office of Science. Los Alamos National Laboratory, an affirmative action equal opportunity employer, is operated by Los Alamos National Security, LLC, for the National Nuclear Security Administration of the U.S. Department of Energy under contract DE-AC52-06NA25396.

References

1. Özkar, S., & Finke, R. G. Palladium(0) Nanoparticle Formation, Stabilization, and Mechanistic Studies: Pd(acac)2 as a Preferred Precursor, [Bu4N]2HPO4 Stabilizer, plus the Stoichiometry, Kinetics, and Minimal, Four-Step Mechanism of the Palladium Nanoparticle Formation and Subsequent Agglomeration Reactions. *Langmuir.* **32** (15), 3699-3716 (2016).
2. Ma, S., Tang, Y., Liu, J., & Wu, J. Visible paper chip immunoassay for rapid determination of bacteria in water distribution system. *Talanta.* **120** 135-140 (2014).
3. Jing, C. *et al.* New insights into electrocatalysis based on plasmon resonance for the real-time monitoring of catalytic events on single gold nanorods. *Analytical chemistry.* **86** (11), 5513-5518 (2014).
4. Tobias, A., Qing, S., & Jones, M. Synthesis, Characterization, and Functionalization of Hybrid Au/CdS and Au/ZnS Core/Shell Nanoparticles. *Journal of Visualized Experiments.* (109), e53383-e53383 (2016).
5. Rezvantalab, H., Connington, K. W., & Shojaei-Zadeh, S. Shear-induced interfacial assembly of Janus particles. *Physical Review Fluids.* **1** (7), 074205 (2016).

6. Mer, V. K. L. Nucleation in Phase Transitions. *Industrial & Engineering Chemistry.* **44** (6), 1270-1277 (1952).
7. LaMer, V. K., & Dinegar, R. H. Theory, production and mechanism of formation of monodispersed hydrosols. *Journal of the American Chemical Society.* **72** (11), 4847-4854 (1950).
8. Polte, J. Fundamental growth principles of colloidal metal nanoparticles-a new perspective. *CrystEngComm.* **17** (36), 6809-6830 (2015).
9. Sugimoto, T., Shiba, F., Sekiguchi, T., & Itoh, H. Spontaneous nucleation of monodisperse silver halide particles from homogeneous gelatin solution I: silver chloride. *Colloids and Surfaces A: Physicochemical and Engineering Aspects.* **164** (2), 183-203 (2000).
10. Yao, Q. *et al.* Understanding seed-mediated growth of gold nanoclusters at molecular level. *Nature Communications.* **8** (2017).
11. van Embden, J., Sader, J. E., Davidson, M., & Mulvaney, P. Evolution of Colloidal Nanocrystals: Theory and Modeling of their Nucleation and Growth. *The Journal of Physical Chemistry C.* **113** (37), 16342-16355 (2009).
12. Vreeland, E. C. *et al.* Enhanced Nanoparticle Size Control by Extending LaMer's Mechanism. *Chemistry of Materials.* **27** (17), 6059-6066 (2015).
13. Watzky, M. A., & Finke, R. G. Transition Metal Nanocluster Formation Kinetic and Mechanistic Studies. A New Mechanism When Hydrogen Is the Reductant: Slow, Continuous Nucleation and Fast Autocatalytic Surface Growth. *Journal of the American Chemical Society.* **119** (43), 10382-10400 (1997).
14. Mozaffari, S. *et al.* Colloidal nanoparticle size control: experimental and kinetic modeling investigation of the ligand-metal binding role in controlling the nucleation and growth kinetics. *Nanoscale.* **9** (36), 13772-13785 (2017).
15. Karim, A. M. *et al.* Synthesis of 1 nm Pd Nanoparticles in a Microfluidic Reactor: Insights from in Situ X-ray Absorption Fine Structure Spectroscopy and Small-Angle X-ray Scattering. *The Journal of Physical Chemistry C.* **119** (23), 13257-13267 (2015).
16. Ortiz, N., & Skrabalak, S. E. Manipulating local ligand environments for the controlled nucleation of metal nanoparticles and their assembly into nanodendrites. *Angewandte Chemie International Edition.* **51** (47), 11757-11761 (2012).
17. Ortiz, N., Hammons, J. A., Cheong, S., & Skrabalak, S. E. Monitoring Ligand-Mediated Growth and Aggregation of Metal Nanoparticles and Nanodendrites by *In Situ* Synchrotron Scattering Techniques. *ChemNanoMat.* **1** (2), 109-114 (2015).
18. Abellan, P. *et al.* Gaining Control over Radiolytic Synthesis of Uniform Sub-3-nanometer Palladium Nanoparticles: Use of Aromatic Liquids in the Electron Microscope. *Langmuir.* **32** (6), 1468-1477 (2016).
19. Yin, X. *et al.* Quantitative Analysis of Different Formation Modes of Platinum Nanocrystals Controlled by Ligand Chemistry. *Nano Letters.* **17** (10), 6146-6150 (2017).
20. Besson, C., Finney, E. E., & Finke, R. G. A Mechanism for Transition-Metal Nanoparticle Self-Assembly. *Journal of the American Chemical Society.* **127** (22), 8179-8184 (2005).
21. Yao, S. *et al.* Insights into the Formation Mechanism of Rhodium Nanocubes. *The Journal of Physical Chemistry C.* **116** (28), 15076-15086 (2012).
22. Asakura, H. *et al.* In situ time-resolved DXAFS study of Rh nanoparticle formation mechanism in ethylene glycol at elevated temperature. *Physical Chemistry Chemical Physics.* **14** (9), 2983-2990 (2012).
23. Harada, M., & Ikegami, R. In Situ Quick X-ray Absorption Fine Structure and Small-Angle X-ray Scattering Study of Metal Nanoparticle Growth in Water-in-Oil Microemulsions during Photoreduction. *Crystal Growth & Design.* **16** (5), 2860-2873 (2016).
24. Lazzari, S., Abolhasani, M., & Jensen, K. F. Modeling of the formation kinetics and size distribution evolution of II-VI quantum dots. *Reaction Chemistry & Engineering.* **2** (4), 567-576 (2017).
25. Maceiczyk, R. M., & Bezinge, L. Kinetics of nanocrystal synthesis in a microfluidic reactor: theory and experiment. *Reaction Chemistry & Engineering.* **1** (3), 261-271 (2016).
26. LaGrow, A. P., Ingham, B., Toney, M. F., & Tilley, R. D. Effect of Surfactant Concentration and Aggregation on the Growth Kinetics of Nickel Nanoparticles. *The Journal of Physical Chemistry C.* **117** (32), 16709-16718 (2013).
27. Lim, B. *et al.* Shape-controlled synthesis of Pd nanocrystals in aqueous solutions. *Advanced Functional Materials.* **19** (2), 189-200 (2009).
28. Schrader, I., Warneke, J., Backenköhler, J., & Kunz, S. Functionalization of Platinum Nanoparticles with l-Proline: Simultaneous Enhancements of Catalytic Activity and Selectivity. *Journal of the American Chemical Society.* **137** (2), 905-912 (2015).
29. Wan, X.-K., Wang, J.-Q., Nan, Z.-A., & Wang, Q.-M. Ligand effects in catalysis by atomically precise gold nanoclusters. *Science Advances.* **3** (10), e1701823 (2017).
30. Yang, Z., & Klabunde, K. J. Synthesis of nearly monodisperse palladium (Pd) nanoparticles by using oleylamine and trioctylphosphine mixed ligands. *Journal of Organometallic Chemistry.* **694** (7), 1016-1021 (2009).
31. Wikander, K., Petit, C., Holmberg, K., & Pileni, M.-P. Size control and growth process of alkylamine-stabilized platinum nanocrystals: a comparison between the phase transfer and reverse micelles methods. *Langmuir.* **22** (10), 4863-4868 (2006).
32. Rempel, J. Y., Bawendi, M. G., & Jensen, K. F. Insights into the Kinetics of Semiconductor Nanocrystal Nucleation and Growth. *Journal of the American Chemical Society.* **131** (12), 4479-4489 (2009).
33. Perala, S. R. K., & Kumar, S. On the Mechanism of Metal Nanoparticle Synthesis in the Brust-Schiffrin Method. *Langmuir.* **29** (31), 9863-9873 (2013).
34. Dreiss, C. A., Jack, K. S., & Parker, A. P. On the absolute calibration of bench-top small-angle X-ray scattering instruments: a comparison of different standard methods. *Journal of applied crystallography.* **39** (1), 32-38 (2006).
35. Li, T., Senesi, A. J., & Lee, B. Small Angle X-ray Scattering for Nanoparticle Research. *Chemical Reviews.* **116** (18), 11128-11180 (2016).
36. Kotlarchyk, M., Stephens, R. B., & Huang, J. S. Study of Schultz distribution to model polydispersity of microemulsion droplets. *The Journal of Physical Chemistry.* **92** (6), 1533-1538 (1988).
37. Watzky, M. A., Finney, E. E., & Finke, R. G. Transition-Metal Nanocluster Size vs Formation Time and the Catalytically Effective Nucleus Number: A Mechanism-Based Treatment. *Journal of the American Chemical Society.* **130** (36), 11959-11969 (2008).
38. Watzky, M. A., & Finke, R. G. Nanocluster Size-Control and "Magic Number" Investigations. Experimental Tests of the "Living-Metal Polymer" Concept and of Mechanism-Based Size-Control Predictions Leading to the Syntheses of Iridium(0) Nanoclusters Centering about Four Sequential Magic Numbers. *Chemistry of Materials.* **9** (12), 3083-3095 (1997).
39. Özkar, S., & Finke, R. G. Nanoparticle Nucleation Is Termolecular in Metal and Involves Hydrogen: Evidence for a Kinetically Effective Nucleus of Three {Ir3H2x·P2W15Nb3O62}6- in Ir(0)n Nanoparticle Formation From [(1,5-COD)Irl·P2W15Nb3O62]8- Plus Dihydrogen. *Journal of the American Chemical Society.* **139** (15), 5444-5457 (2017).
40. Sahu, P., & Prasad, B. L. Time and temperature effects on the digestive ripening of gold nanoparticles: is there a crossover from digestive ripening to Ostwald ripening? *Langmuir.* **30** (34), 10143-10150 (2014).

41. Schwartzkopf, M. *et al.* Real-Time Monitoring of Morphology and Optical Properties during Sputter Deposition for Tailoring Metal-Polymer Interfaces. *ACS Applied Materials & Interfaces.* **7** (24), 13547-13556 (2015).

